Membrane dynamics during cellular wound repair

Nicholas R. Davenport[a], Kevin J. Sonnemann[b], Kevin W. Eliceiri[b,c], and William M. Bement[a,b,d,*]
[a]Program in Cellular and Molecular Biology, [b]Laboratory of Cell and Molecular Biology, [c]Laboratory for Optical and Computational Instrumentation, and [d]Department of Zoology, University of Wisconsin–Madison, Madison, WI 53706

ABSTRACT **Cells rapidly reseal after damage, but how they do so is unknown. It has been hypothesized that resealing occurs due to formation of a patch derived from rapid fusion of intracellular compartments at the wound site. However, patching has never been directly visualized. Here we study membrane dynamics in wounded *Xenopus laevis* oocytes at high spatiotemporal resolution. Consistent with the patch hypothesis, we find that damage triggers rampant fusion of intracellular compartments, generating a barrier that limits influx of extracellular dextrans. Patch formation is accompanied by compound exocytosis, local accumulation and aggregation of vesicles, and rupture of compartments facing the external environment. Subcellular patterning is evident as annexin A1, dysferlin, diacylglycerol, active Rho, and active Cdc42 are recruited to compartments confined to different regions around the wound. We also find that a ring of elevated intracellular calcium overlaps the region where membrane dynamics are most evident and persists for several minutes. The results provide the first direct visualization of membrane patching during membrane repair, reveal novel features of the repair process, and show that a remarkable degree of spatial patterning accompanies damage-induced membrane dynamics.**

Monitoring Editor
David G. Drubin
University of California, Berkeley

Received: Apr 11, 2016
Revised: May 17, 2016
Accepted: May 18, 2016

INTRODUCTION

The capacity for self-repair is an essential trait of both individual cells and multicellular organisms. Not only do cells frequently incur plasma membrane disruptions large enough to warrant repair to prevent loss of cytoplasm or induction of proteolytic pathways by influx of extracellular calcium (McNeil and Ito, 1989), but also the inability of cells to mount a sufficient repair response is linked to a variety of disease states, including diabetes (Howard *et al.*, 2011), muscular dystrophies (Bansal *et al.*, 2003), and vitamin deficiencies (Labazi *et al.*, 2015).

Although our understanding of cell repair is fragmentary, work on several different systems indicates that in most if not all eukaryotic cells it hinges on at least two complementary, calcium-dependent pathways: a "resealing" response that limits exchange between the cytoplasm and the extracellular environment (Steinhardt *et al.*, 1994; Terasaki *et al.*, 1997; Cooper and McNeil, 2015), and a cytoskeletal response in which the small GTPases Rho, Rac, and Cdc42 coordinate the assembly and closure of an F-actin and myosin-2 contractile array at the wound site (Mandato and Bement, 2001; Benink and Bement, 2005; Abreu-Blanco *et al.*, 2011, 2014).

Although there is consensus that the resealing event is critically important, exactly how it occurs is the subject of controversy. Perhaps the most parsimonious idea is the "patch" hypothesis, in which calcium-dependent fusion of intracellular compartments with each other and with the plasma membrane generates a continuous membrane patch at the site of cell damage (Terasaki *et al.*, 1997; McNeil *et al.*, 2000). The patch hypothesis is supported by several lines of evidence, including the demonstration that sea water injected into a sea urchin egg is rapidly walled off from the surrounding cytoplasm (Terasaki *et al.*, 1997) and the demonstration that cell repair requires internal membrane compartments (McNeil *et al.*, 2003).

Fusion of internal compartments with each other has never been directly observed at sites of cell damage, however, and this and other considerations have led some to question whether patching actually occurs (Andrews and Perez, 2015). Further, several other resealing mechanisms have been proposed (reviewed in

This article was published online ahead of print in MBoC in Press (http://www.molbiolcell.org/cgi/doi/10.1091/mbc.E16-04-0223) on May 25, 2016.

*Address correspondence to: William Bement (wmbement@wisc.edu).

Abbreviations used: BFP, blue fluorescent protein; C1, C1 domain of PKCβ; C2, C2 domain of PKCβ; DAG, diacylglycerol; eGFP, enhanced green fluorescent protein; FM 1-43, *N*-(3-triethylammoniumpropyl)-4-(4-(dibutylamino)styryl)pyridinium dibromide; PKCβ, protein kinase C β; PM, plasma membrane; R18, octadecyl rhodamine B chloride.

© 2016 Davenport *et al.* This article is distributed by The American Society for Cell Biology under license from the author(s). Two months after publication it is available to the public under an Attribution–Noncommercial–Share Alike 3.0 Unported Creative Commons License (http://creativecommons.org/licenses/by-nc-sa/3.0).

"ASCB®," "The American Society for Cell Biology®," and "Molecular Biology of the Cell®" are registered trademarks of The American Society for Cell Biology.

Moe *et al.*, 2015), including exocytosis (Steinhardt *et al.*, 1994; Bi *et al.*, 1995; Miyake and McNeil, 1995; Reddy *et al.*, 2001), endocytosis (Idone *et al.*, 2008), membrane excision (Jimenez *et al.*, 2014), and plugging of membrane holes via compartment aggregates (Eddleman *et al.*, 1997).

One of the major reasons our understanding of membrane resealing is limited in spite of its obvious importance is that the majority of analyses monitoring the dynamics of membranes after wounding have been performed at relatively low spatiotemporal resolution. To address this deficit, we used a series of general and specific probes for lipids, proteins, and intracellular signals with high-speed, high-resolution confocal imaging to characterize the membrane dynamics elicited by plasma membrane damage of *Xenopus* oocytes, which have a robust and readily observable wound response (Bement *et al.*, 1999). Using this approach, we provide the first direct visualization of patching. We also find that wounding elicits compound exocytosis and a novel behavior that we term "explodosis" in which membranous compartments rupture outward at the wound site. Further, we find that patching is accompanied by accretion of membranous compartments in association with two proteins previously implicated in cell repair—annexin and dysferlin—as well as the small GTPases Rho and Cdc42 in distinct subcellular patterns around wounds. Finally, we find that intracellular calcium remains locally elevated around wounds for several minutes in a region overlapping the contractile array used to reestablish the integrity of the cytoskeleton.

RESULTS

Live imaging of cell repair comes with several inherent challenges. First, repair is very rapid, commencing within 1 s or so of damage; second, the wound itself is a moving target, as actomyosin-powered contraction brings the edges of the wound together beginning at ~30–60 s postwounding; third, what is observed depends on the focal plane and the angle of imaging; and fourth, what is seen also depends on the probe used. To overcome these challenges, we used several different imaging approaches—standard laser scanning confocal microscopy of single focal planes or, occasionally, *z*-stacks; fast swept field confocal microscopy of *z*-stacks; and use of two different imaging angles for single focal planes—en face (i.e., looking directly down on the wound) and oblique (i.e., wounding an area where the oocyte surface curves away from the coverslip so that regions both below and at the level of the plasma membrane can be viewed in the same plane). We combined these imaging approaches with several different probes, both generic and specific, for membranes, ions, and proteins. All of the membrane dynamics described here were observed with a minimum of two different probes; some (e.g., exocytosis and patching) were seen with three or more.

Wounding triggers exocytosis and formation of large membrane compartments at wound sites

Wounding of sea urchin eggs triggers local exocytosis of cortical secretory granules (cortical granules; Bi *et al.*, 1995; Miyake and McNeil, 1995). It seemed unlikely that cortical granule exocytosis would also be triggered by wounding in frog oocytes, in that exocytosis in oocytes (in contrast to eggs, a later meiotic stage) is refractory to elevation of intracellular calcium (reviewed in Bement, 1992). Nonetheless, we tested this possibility by wounding oocytes in the presence of external dextran, which labels exocytosing cortical granules by incorporating into their lumen after they release their contents (Sokac *et al.*, 2003). In spite of our expectations, wounding not only resulted in a rapid incorporation of dextran that was largely confined to the immediate wound site (Figure 1A, arrowheads; see also later discussion), it also triggered progressive exocytosis of cortical granules up to ~15 µm distal to the wound site (Figure 1A and Supplemental Movie S1).

As an alternative to dextran, we assessed exocytosis using *N*-(3-triethylammoniumpropyl)-4-(4-(dibutylamino)styryl)pyridinium dibromide (FM 1-43), a cell-impermeant, lipophilic dye that is often used to study membrane repair; its fluorescence emission increases upon incorporation into hydrophobic environments. Fast imaging series (1- to 2-s time points) at the plane of the plasma membrane revealed exocytotic events as transient openings in the FM 1-43–stained plasma membrane (PM; Figure 1B and Supplemental Movie S2). In oblique views of oocyte wounds, FM 1-43 revealed an additional feature of the wound response: accumulation of large, dynamic membranous compartments in the center of the wound (Figure 1C and Supplemental Movie S3).

Fusion of intracellular compartments at wound sites to generate a patch

The rapid confinement of dextran to the immediate wound site and the formation of large, FM 1-43–staining compartments at wounds hinted at the possibility that dextran spreading might be limited by fusion of internal compartments—that is, patch formation. However, FM 1-43, while readily staining the plasma membrane, cell surface projections, and other external structures at wound sites, did not effectively label internal compartments of the oocyte before wounding, even when microinjected (unpublished data). We therefore wounded oocytes in the presence of dextran after staining with octadecyl rhodamine B chloride (R18), a nonspecific membrane dye. R18 labeled both the PM (unpublished data) and, based on their size, distribution, and abundance (Campanella and Andreuccetti, 1977; see later discussion) the cortical granules (Figure 2 and Supplemental Movie S4). Immediately after wounding, the wound area contained dextran but was largely devoid of cortical granules (Figure 2 and Supplemental Movie S4). Dextran did not appear to diffuse away from the initial wound site but instead either remained constrained by tightly opposed cortical granules or spread incrementally in a manner suggestive of local membrane fusion or disruption (Figure 2, top, and Supplemental Movie S4; see also later discussion). Indeed, higher-magnification views showed that R18-labeled compartments could first fuse with each other, forming a larger compartment, and then subsequently incorporate dextran after apparently rupturing on the side bordering the dextran (Figure 2, bottom; enlargement 1) or undergo rupture and dextran incorporation without a prior fusion event (Figure 2, bottom; enlargement 2).

Although these results showed that endogenous, membrane-bound compartments—the cortical granules—participate in the repair process, further analysis of repair dynamics was hampered by the fact that the R18 was rapidly lost from cortical granules facing the wound edge. We therefore used a fusion protein comprising enhanced green fluorescent protein (eGFP) fused to the C2 domain of protein kinase C β (PKCβ; eGFP-C2), which binds to phosphatidylserine in the presence of elevated calcium and was previously shown to provide high-contrast labeling of cortical granules after calcium elevation (Yu and Bement, 2007). The combination of R18, eGFP-C2, and dextran allowed us to track the fate of cortical granules at wound sites: upon wounding, multiple R18-labeled compartments rapidly fuse, forming a compartment within which the dextran is contained (Figure 3 and Supplemental Movie S5). The C2 probe is rapidly recruited to the membrane of this compartment even as the R18 is lost and is retained there for ~10–60 s, providing a high-contrast label of a continuous membrane layer that forms around the

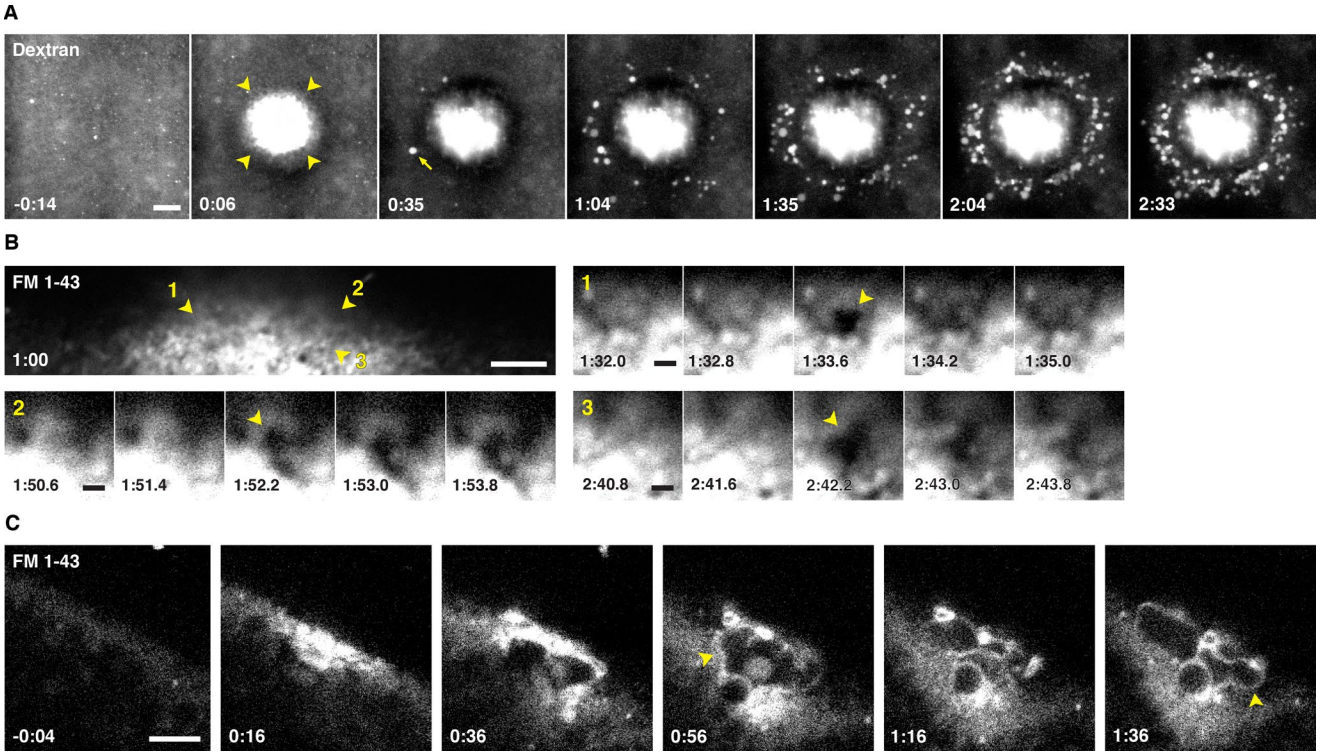

FIGURE 1: Exocytosis occurs upon wounding. (A) *X. laevis* oocyte wounded in the presence of extracellular fluorescent dextran (Texas Red dextran). Intrusion of dextran into the cell is initially limited to a region proximal to the wound (arrowheads), but then compartments distal to the wound undergo exocytosis and imbibe dextran (first event indicated by arrow). See Supplemental Movie S1. (B) An oblique view of an oocyte wounded in medium containing FM 1-43. Wound center is out of frame, toward the bottom of the image. Numbered arrowheads indicate sites of exocytosis, highlighted in enlarged insets. See Supplemental Movie S2. (C) Oblique view of an oocyte wounded in the presence of FM 1-43. Arrowheads highlight membranous compartments labeled by FM 1-43 during repair. See Supplemental Movie S3. Times in minutes:seconds, with $t = 0:00$ corresponding to moment of wounding. Scale bars, 10 μm (A), 5 μm (B, C), 1 μm (B, insets).

wound site. Further, the membrane labeled with C2 is contiguous with the plasma membrane, which retains R18 labeling (Figure 3; $t = 0:04–0:08$). Because this result is exactly what is predicted by the patch hypothesis, we will refer to the membranous structure that bounds the wound site as the "patch."

Patching dynamics

The high signal:noise provided by eGFP-C2 permitted us to analyze the patching process in more detail. Patches begin forming within several seconds of wounding and thereafter undergo essentially constant remodeling (Figure 4A and Supplemental Movie S6). Specifically, on the immediate outside of the patch (i.e., in the extracellular space), strange, extremely dextran-rich structures grew slowly from the patch floor in a manner that frustrated all of our efforts at characterization. Further, the cytoplasmic region surrounding the patch accumulated membranous compartments, many of which become cross-linked with the patch and/or each other, as judged by accumulation of C2 probe at sites of contact and distortion of compartment shape (Figure 4, A′ and B, and Supplemental Movies S6 and S7). The dextran remained confined to the exoplasmic side of the regions where compartments were tightly packed, even in the absence of a continuously labeled (with eGFP-C2) patch, suggesting that the packing was sufficient to form a barrier impermeable to dextran influx (e.g., Figure 4A′).

The patch also served as a site of extensive membrane fusion. For example, the cytoplasmic compartments immediately abutting the patch often fused with it and then each other, as judged by dextran incorporation (Figure 4, A and B, and Supplemental Movies S6 and S7). Most of the compartments involved were likely cortical granules, based on their size and intense labeling with eGFP-C2; much smaller, C2-poor compartments were also observed, however, reminding us that there may be many other compartments participating that are not labeled with the probes being used (Figure 4, C and C′).

The patch served as a site of compound exocytosis, with an initial fusion event being followed by one or more fusions with deeper (in the cytoplasm) compartments (Figure 5A and Supplemental Movie S8). However, there did not appear to be a strict requirement for prior union with a PM-containing compartment (i.e., either the PM itself or a compartment that had previously fused with the PM), in that eGFP-C2-labeled compartments were occasionally observed to fuse with each other first and then fuse with dextran-containing compartments (Figure 5B and Supplemental Movie S9; see also Figure 2).

Explodosis

The foregoing results provided a paradox: wounding clearly elicits local fusion of intracellular compartments, which is expected to generate large, completely membrane-enclosed compartments at the wound site, and yet the patching membrane often appears to have no "roof"—that is, it seems to be a single bilayer (e.g., Figure 4). The apparent rupture of the R18-labeled compartments observed in Figure 2 suggested a resolution to this paradox—compartments

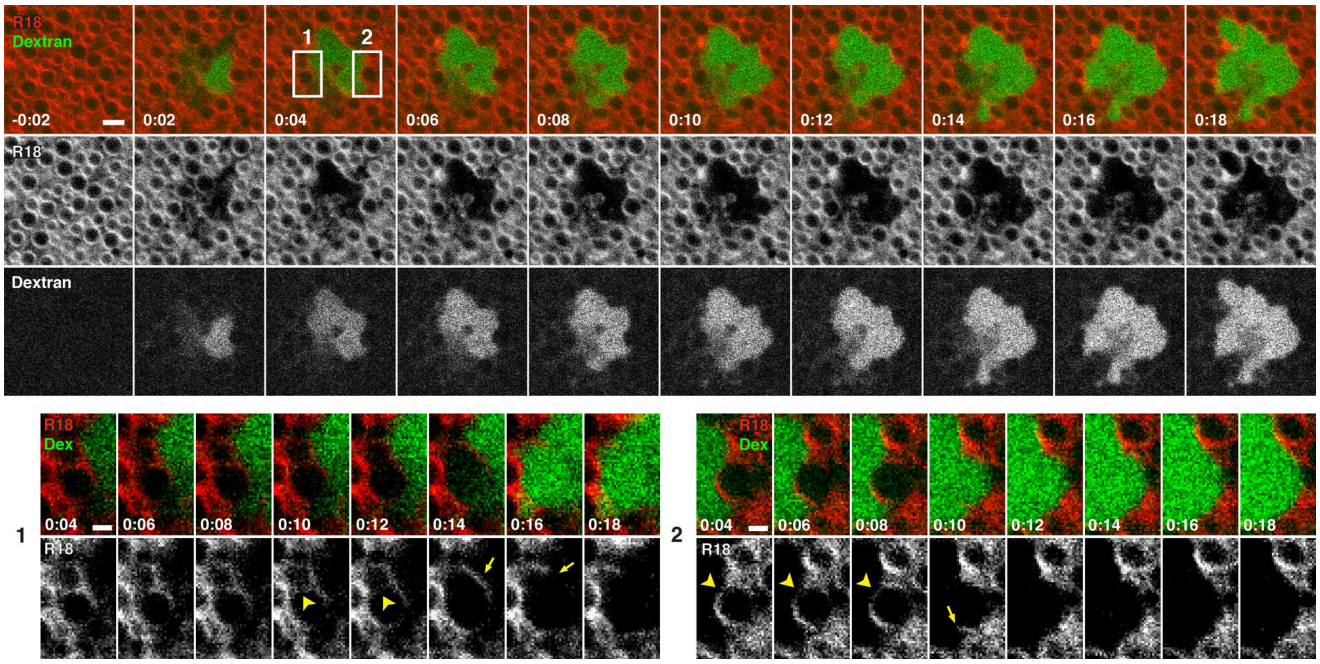

FIGURE 2: Extracellular dextran has limited access to the cytoplasm of wounded cells. En face view of oocyte prestained with R18 and wounded in the presence of extracellular fluorescent dextran (Oregon Green 488 dextran). Areas highlighted by boxes at $t = 0:04$ are enlarged to highlight wound dynamics. Enlargement of region 1 (bottom, left) shows fusion of two compartments (arrowheads) before rupture and imbibing of dextran at 0:14–0:16. Arrow shows fragment of compartment after rupture. Enlargement of region 2 (bottom, right) highlights a compartment at the wound edge (arrowheads) that is exposed to dextran upon rupture at 0:10. A fragment of the vesicle is visible after rupture (arrow). See Supplemental Movie S4. Times in minutes:seconds, with $t = 0:00$ corresponding to moment of wounding. Scale bars, 5 μm (top), 2.5 μm (bottom).

exposed to the extracellular medium might rupture outward. Consistent with this mechanism, oblique, single-optical-plane movies of repair in eGFP-C2–labeled cells revealed that compartments facing the extracellular environment often popped open and then collapsed into a single membrane (Figure 6, A and A′, and Supplemental Movie S10). To better visualize this process in *x*, *y*, and *z* over time, we took advantage of the superior speed provided by swept field confocal microscopy (Bembenek *et al.*, 2007; Castellano-Muñoz *et al.*, 2012; Ponomareva *et al.*, 2016), which permits 12–20 *z*-plane stacks to be captured in 2 s (Figure 6, B and B′, and Supplemental Movies S11–S13). Figure 6, B and B′ (also see Supplemental Movies S12 and S13), shows a series in which three small compartments first fuse with each other, forming a large, continuous compartment that subsequently ruptures on the side facing the outside of the cell. Because this behavior is fairly violent and appears qualitatively different from other behaviors previously described, we refer to it as "explodosis."

Human annexin A1 and dysferlin are rapidly recruited to membrane compartments around wounds

Annexins have been implicated in cell repair in several systems (McNeil *et al.*, 2006; Potez *et al.*, 2011; Swaggart *et al.*, 2014). To obtain insight into their potential roles in this process and assess the potential of the oocyte system for heterologous analysis of human repair proteins, we generated an eGFP-human annexin A1 fusion (eGFP-annexin) and expressed it in oocytes. Low-magnification, en face movies showed rapid recruitment of eGFP-annexin to wounds, where it localized to the PM in a tight ring bordering the wound and to membranous compartments both beneath the wound and on the interior of the wound region (Figure 7A and Supplemental Movie S14). High-magnification movies revealed that eGFP-annexin was recruited to small foci around wounds within 2–4 s (Figure 7B and Supplemental Movie S15; also unpublished data). Recruitment of eGFP-annexin to vesicles often preceded incorporation of dextran (Figure 7B and Supplemental Movie S15), indicating that there is no requirement for PM–compartment fusion for annexin recruitment. Further, we observed few if any cases of fusion of compartments around the wound edge that were not eGFP-annexin labeled, suggesting the possibility that annexin might participate in the fusion process (see *Discussion*). Movies made from oblique views often revealed discontinuous localization of eGFP-annexin on the "floor" of the wound site, consistent with it being a component of the patch (Figure 7, C and C′, and Supplemental Movie S16). However, this localization was typically transient (Supplemental Movie S16), suggesting that, once formed, the patch is continually remodeled.

To extend the analysis of heterologous protein targeting to wounds, we assessed the dynamics of human dysferlin, a protein implicated in repair of skeletal muscle (Bansal *et al.*, 2003; Lennon *et al.*, 2003). The size of eGFP-dysferlin (~265 kDa; mRNA of ~7 kb) precluded the use of in vitro–transcribed mRNA. We therefore expressed eGFP-human dysferlin (eGFP-dysferlin) in insect cells and purified it to homogeneity (Figure 7D). After injection into oocytes, eGFP-dysferlin was cytoplasmic. However, upon wounding, it was recruited to both the plasma membrane and intracellular compartments at the wound (Figure 7, E and E′). Like eGFP-annexin, eGFP-dysferlin was localized to a tight ring on the PM around the wound; unlike eGFP-annexin, eGFP-dysferlin did not extensively label all of the large compartments within the wound (Figure 7, E and E′).

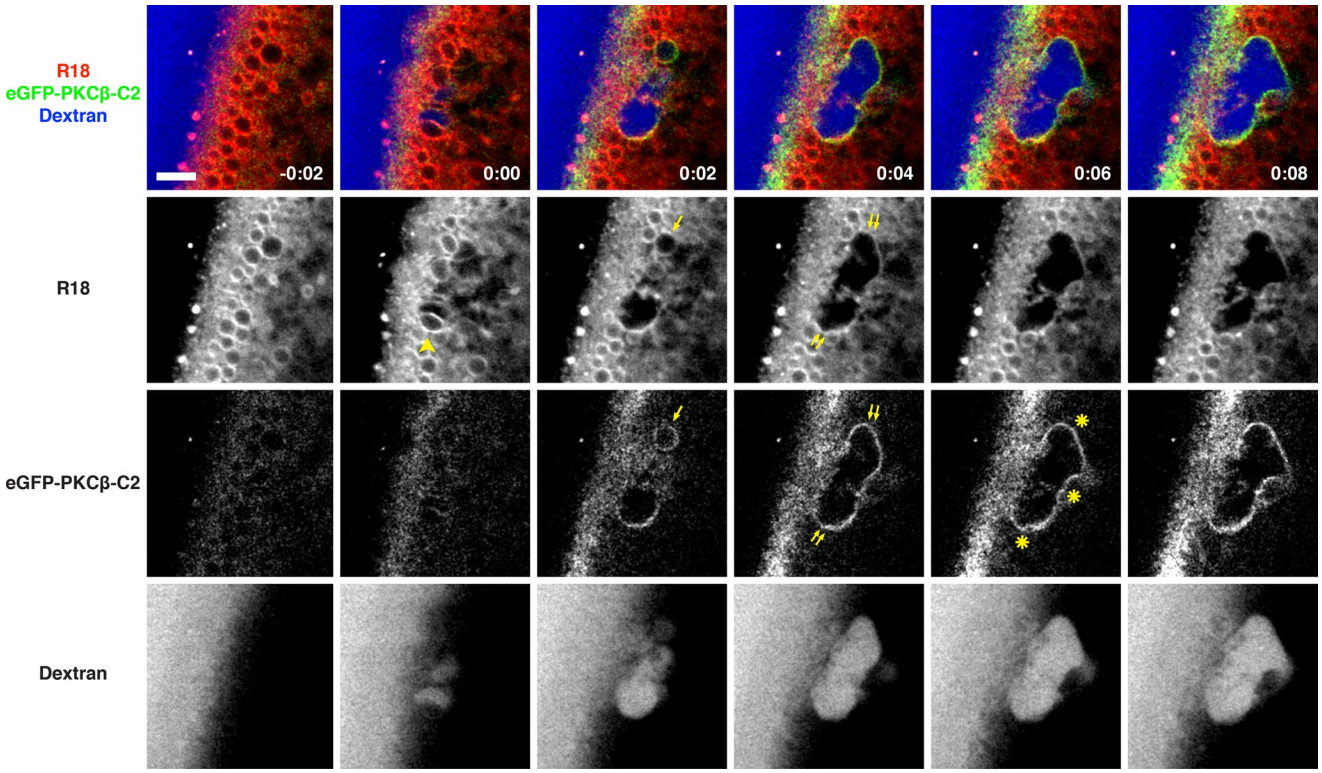

FIGURE 3: Vesicle–vesicle fusion at sites of plasma membrane disruption. An oocyte expressing eGFP-PKCβ-C2 (a probe for phosphatidylserine and calcium) was preincubated with R18 and wounded in the presence of fluorescent extracellular dextran (Alexa Fluor 647 dextran). Arrowhead at $t = 0:00$ denotes R18-labeled vesicle about to undergo fusion. eGFP-C2 probe begins to label R18-stained compartments (arrow at $t = 0:02$) soon after wounding. eGFP-C2–labeled compartment is contiguous with the plasma membrane (double arrows) and forms a barrier (asterisks) limiting dextran influx. See Supplemental Movie S5. Time in minutes:seconds, with $t = 0:00$ corresponding to the moment of wounding. Scale bar, 5 μm.

Membrane remodeling continues long after initial PM damage

It was evident from the foregoing results that the wound response continued well after the first minute of wounding. However, it was also evident that several of the probes—R18, eGFP-C2, and eGFP-annexin—were often lost from a given membranous structure over time. We therefore analyzed wound dynamics using the C1 domain of PKCβ fused to eGFP (eGFP-C1). This probe binds specifically to diacylglycerol (DAG), a signaling lipid previously shown to be generated at wound sites, to persist at wounds for several minutes, and to be required for proper wound repair (Vaughan *et al.*, 2014). eGFP-C1 accumulated around wounds in a tight ring at the plasma membrane and also accumulated on membranous compartments around the wound site (Figure 8A and Supplemental Movie S17; also unpublished data). Double labeling with mRFP-C1 and eGFP-C2 revealed that the PM DAG is initially concentrated within a broader ring defined by the eGFP-C2 probe (Figure 8B and Supplemental Movie S18). Strikingly, whereas the eGFP-C2 signal wanes over the course of several minutes, eGFP-C1 remains concentrated on the PM and on membranous compartments underneath the wounds for at least 15 min (Figure 8C and Supplemental Movie S19; also unpublished data). The DAG-labeled compartments are highly dynamic, and their behavior suggests that the wound response continues long after the initial healing is largely finished (Figure 8C and Supplemental Movie S19).

C2 recruitment parallels increases in intracellular free calcium

In principle, targeting of the C2 domain to the wound site, as well as its eventual loss, could reflect changes in intracellular free calcium, changes in phosphatidylserine distribution, or both. However, previous results showed that although phosphatidylserine becomes more enriched around wound sites over time, this process is not evident until ~90 s postwounding (Vaughan *et al.*, 2014), well after the observed recruitment of eGFP-C2. It therefore seemed likely that the spatiotemporal recruitment pattern of eGFP-C2 was driven by calcium, with the preexisting (i.e., prewounding) membrane phosphatidylserine serving as a passive platform for C2 binding. To test this possibility, we imaged C2 fused with blue fluorescent protein (BFP-C2) together with GCaMP5G, a circularly permuted eGFP construct that has increased fluorescence in the presence of calcium ions (Akerboom *et al.*, 2012). Wounding triggered a rapid (within 1 s) increase in fluorescence signal of GCaMP5G in a broad bloom around wounds (Figure 9 and Supplemental Movie S20; also unpublished data). However, within ~30 s, the bloom decreased rapidly, with the GCaMP5G eventually forming an ~8-μm disk of increased signal around the wound (Figure 9 and Supplemental Movie S20). The disk decreased in size steadily as healing progressed, and the GCaMP5G signal eventually disappeared within ~5 min (Figure 9 and Supplemental Movie S20; also unpublished data). Double labeling showed that BFP-C2 followed a similar pattern, with the following differences: it took ~5–10 s for the BFP-C2 bloom to be

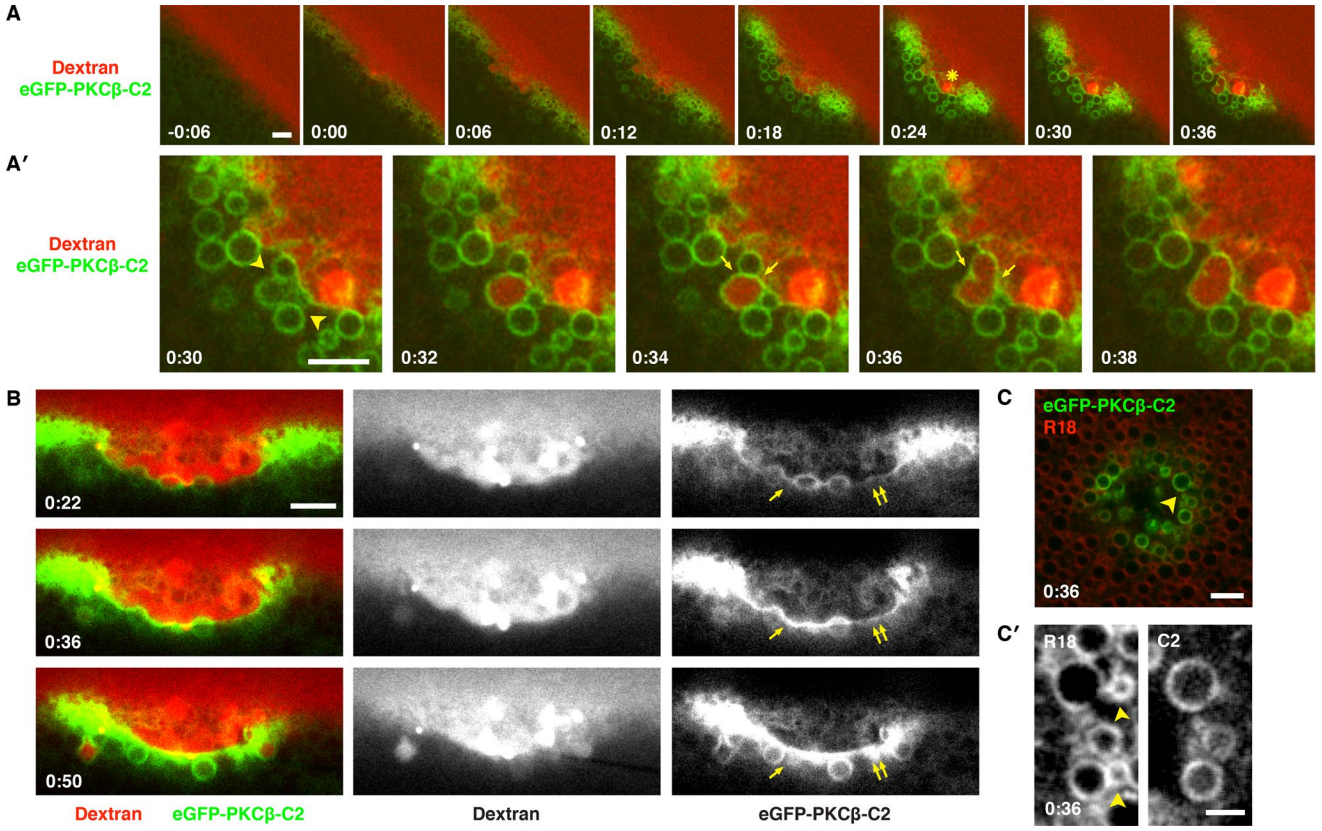

FIGURE 4: The C2 domain of PKCβ labels intracellular vesicles and wound patch. (A) Oblique, low-magnification view of oocyte expressing eGFP-PKCβ-C2 wounded in the presence of extracellular fluorescent dextran (Texas Red dextran). eGFP-PKCβ-C2 is rapidly recruited to the wound and labels vesicles clustered around its edge. A brightly stained structure (asterisk) of unknown identity appears in the wound pit. See Supplemental Movie S6. (A′) Enlargement of A starting at $t = 0:30$, showing tightly packed, C2-labeled vesicles at the wound edge (arrows) closely opposed to a nascent patch (green line bordering wound). A large vesicle fuses with the patch and imbibes dextran (0:32) and then fuses with another vesicle (0:36). (B) Cell expressing eGFP-PKCβ-C2 wounded in the presence of extracellular fluorescent dextran (Texas Red dextran). Single arrowheads denote membranous compartments incorporated into the patch; double arrowheads denote a region of the patch that progressively accumulates C2. See Supplemental Movie S7. (C) Oocyte expressing eGFP-PKCβ-C2 and stained with R18 before wounding. The vesicular structures labeled by the C2 probe upon wounding are also labeled by R18 (arrowhead). (C′) Enlargement of C showing that the C2 probe labels most, but not all, compartments labeled by R18 (R18-labeled vesicles free of C2 signal are denoted by the arrowheads). Times in minutes:seconds, with $t = 0:00$ corresponding to moment of wounding. Scale bars, 5 μm (A, A′, B, C), 2.5 μm (C′).

evident (Figure 9 and Supplemental Movie S20); the area occupied by BFP-C2 was generally less broad than that occupied by GCaMP5G fluorescence (Figure 9); whereas the GCaMP5G signal was diffuse, as expected for a soluble calcium reporter, the BFP-C2 was sharply confined to the PM and on intracellular membrane compartments (Figure 9 and Supplemental Movie S20; see also Figures 3–6). Based on these results, the overall similarity of the timing and pattern of C2 recruitment and GCaMP5G signal, and the known ability of C2 to bind to phosphatidylserine in the presence of elevated calcium (Kohout *et al.*, 2002), it is likely that changes in calcium are the primary driver of C2 recruitment, and, conversely, C2 recruitment represents a reasonable surrogate for elevation of intracellular free calcium.

Patterning of membrane dynamics

Many of the foregoing results hinted at the possibility that the precise pattern formation events previously described at the level of the PM, in which the small GTPases Rho and Cdc42 form concentric zones of activity around each other (Benink and Bement, 2005), might be mirrored in some of the membrane dynamics elicited by wounding. That is, the distinct patterns of C1 and C2 accumulation, the tight focusing of annexin and dysferlin at the wound edge, and differential distribution of dextran-containing compartments (e.g., Figure 1A) hinted that the apparently promiscuous and chaotic membrane fusion events might be subject to more order than is apparent at first glance. In particular, because Rho and Cdc42 have been linked to membrane dynamics in other systems (reviewed in Ridley, 2006), we hypothesized that their activity might not be confined to the PM but might also be localized to the dynamic membrane compartments that form during healing. We first addressed this point by comparing the distribution of elevated intracellular free calcium, Cdc42 activity, and Rho activity using triple labeling with GCaMP5G, BFP-wGBD, and mCherry-2xrGBD (wGBD and rGBD are probes that specifically bind to active Cdc42 and active Rho, respectively; Benink and Bement, 2005). This approach revealed that the formation of the focused disk of intracellular free calcium preceded Rho and Cdc42 activation and that the highest concentration of elevated calcium within the disk precisely overlapped the Rho and the Cdc42 zone once the latter had formed around wounds (Figure 10, A and A′, and Supplemental Movie S21;

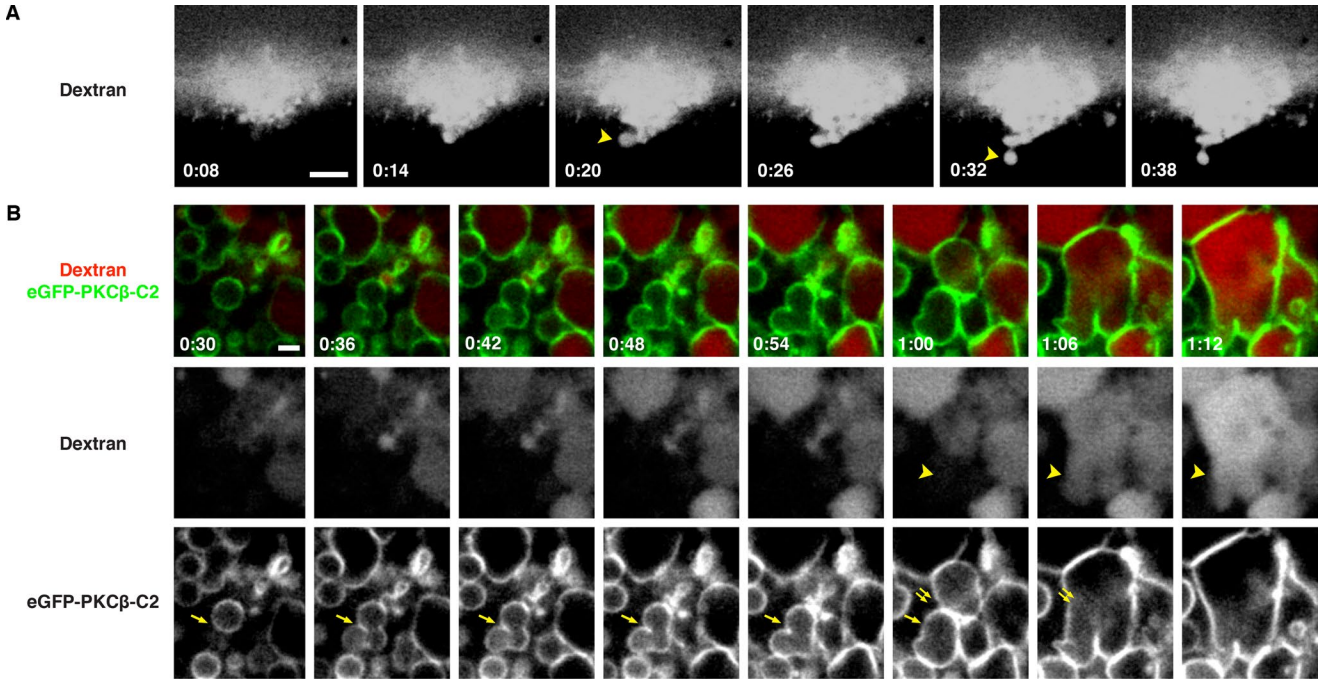

FIGURE 5: Vesicle–vesicle fusion continues through wound repair. (A) Oblique view of oocyte wounded in the presence of extracellular fluorescent dextran (Texas Red dextran) reveals compound exocytosis occurs at the wound edge (i.e., the site of patch formation). Compound exocytotic events are indicated by arrowheads. See Supplemental Movie S8. (B) Oblique, high-magnification view of the edge of a wound in an oocyte expressing eGFP-PKCβ-C2 wounded in the presence of extracellular fluorescent dextran (Alexa Fluor 647 dextran, pseudocolored red). Small, tightly packed vesicles near the wound edge (arrow) acquire C2, fuse with each other (0:48–0:54), and then fuse with another large compartment (double arrows), thereby acquiring dextran (arrowheads). See Supplemental Movie S9. Time in minutes:seconds, with t = 0:00 corresponding to the moment of wounding. Scale bars, 5 μm (A), 2 μm (B).

also unpublished data). Eventually, the Cdc42 activity declined coincident with the fall of intracellular free calcium, whereas Rho activity persisted for much longer. These results, taken in conjunction with those given earlier, indicate that intracellular free calcium, active Rho, and active Cdc42 are all concentrated in the same general region where patching and wound-induced compartment fusion occur and that the dynamics of active Cdc42 parallels that revealed by GCaMP5G and C2, whereas that of Rho parallels the dynamics of C1.

We then used swept field confocal imaging to allow us to follow the dynamics of active Rho and active Cdc42 both at the PM level and much deeper (~3–10 μm) with rapid acquisition (2- to 3-s intervals) during the course of wounding and repair. Imaging at the level of the PM clearly revealed that exocytotic events occur within both of the GTPase zones as they form and that such events continued as the zones close inward (Figure 10B, top, and Supplemental Movie S22). Such grazing views also occasionally revealed membranous compartments that appeared to be squeezed from the wound edge into the center of the wound (Figure 10B, top, and Supplemental Movie S22, bottom).

Remarkably, imaging the region beneath the PM revealed that the concentric pattern of active Rho and active Cdc42 evident at the PM was maintained beneath the PM around the wound, with each active GTPase confined to a different subset of membrane compartments: active Rho concentrated on compartments immediately abutting the wound, whereas active Cdc42 concentrated on compartments more distal to it (Figure 10B, bottom, and Supplemental Movie S23). The two sets of compartments displayed qualitatively different behavior: compartments that harbored active Rho were relatively inert, whereas those associated with active Cdc42 were highly dynamic and displayed rapid shape changes, changes in the intensity of Cdc42 signal, and changes in position (Figure 10B, bottom, and Supplemental Movie S23).

DISCUSSION

In this study, we sought to explain a centuries-old observation: when the surface (PM) of a cell is disrupted, a "film" or barrier layer is quickly erected at the site of damage to prevent loss of cytoplasm (for a review of the early literature, see Heilbrunn, 1928). Electron microscopy (EM) studies suggest that this barrier at least partly comprises membranes (e.g., Gingell, 1970; Bluemink, 1972; Krause *et al.*, 1994; Miyake and McNeil, 1995), and, in keeping with this notion, a variety of membrane-binding proteins and membrane compartments have been implicated in cell repair (Moe *et al.*, 2015). However, the cellular mechanisms that lead to barrier formation have remained elusive, giving rise to a variety of models, including resealing via exocytosis, endocytosis, scission, aggregation, and patching. Our results provide the first direct demonstration of patching: we visualized fusion of internal compartments with each other at the sites of wounds, showed that this results in formation of larger compartments that limit diffusion of fluorescent dextran, and showed that these larger compartments are contiguous with the PM (Figure 11).

Are the observations described here specific to oocytes? That is, are they applicable to other systems, or are they merely a consequence of using a large cell with a readily accessible cache of cortical granules, compartments that undergo calcium-dependent membrane fusion at fertilization? The former possibility seems most congruent with the data. First, as noted, cortical granules in *Xenopus*

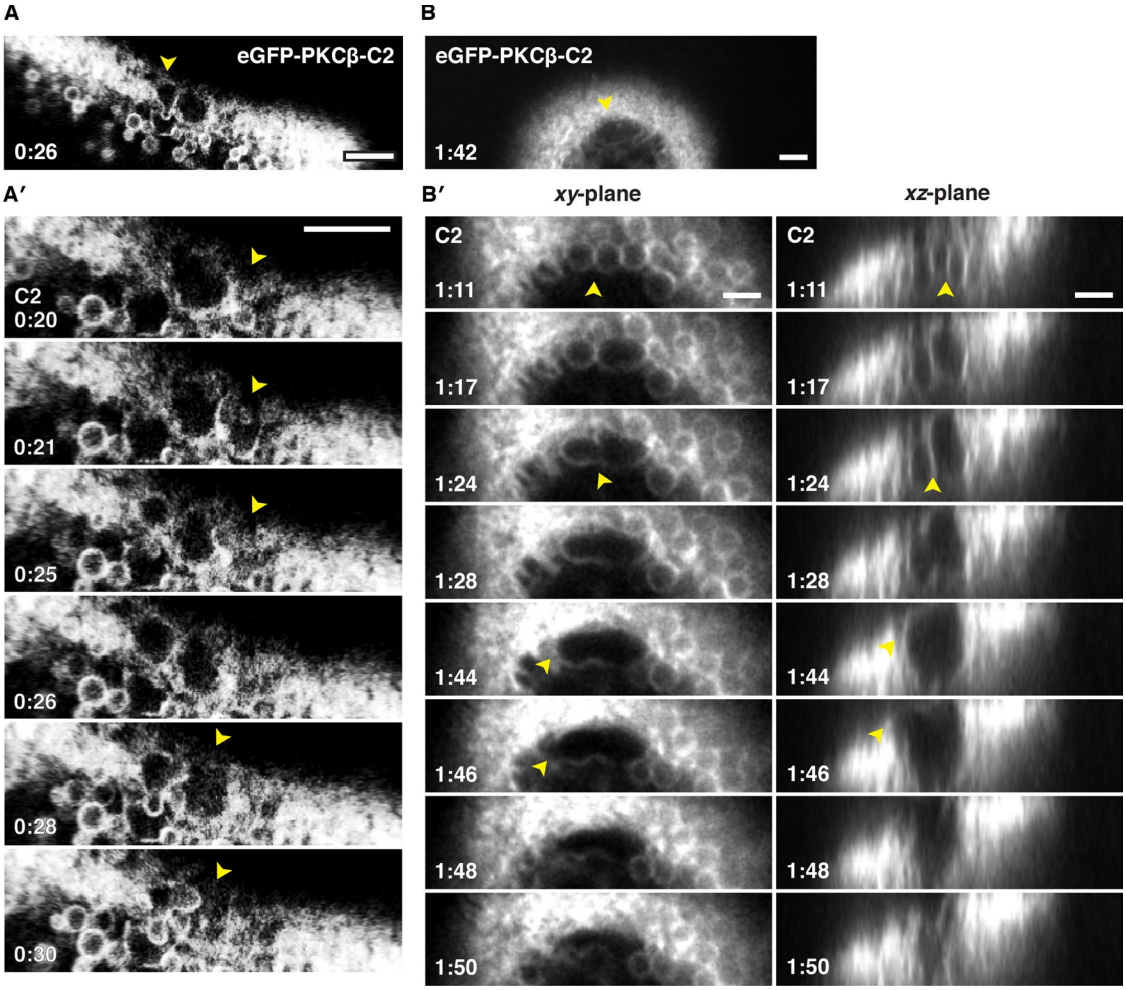

FIGURE 6: High-speed imaging of vesicle–vesicle fusion and rupture. (A) Still from a single-focal plane movie showing an oblique view of wounded oocyte expressing eGFP-PKCβ-C2. (A′) Enlargement and movie series from same wound depicted in A, showing growth, rupture, and collapse of vesicles (arrowhead) at the wound edge. Supplemental Movie S10 shows several cycles of growth, rupture, and collapse of vesicles. (B) Still from a high-resolution four-dimensional movie showing wounded oocyte expressing eGFP-PKCβ-C2 forming a large compartment (arrowheads) at the wound edge that was no longer visible several frames later (not shown). See Supplemental Movie S11. (B′) Enlargement of B along the *xy*- (left) and *xz*-planes (right) reveals fusion of smaller compartments before rupture of the apical portion of membrane and subsequent collapse of the entire compartment. See Supplemental Movies S12 and S13. Time in minutes:seconds, with $t = 0:00$ corresponding to the moment of wounding. Scale bars, 5 μm.

oocytes cannot be stimulated to undergo exocytosis even by exposure to calcium ionophore, a manipulation that triggers rapid exocytosis in *Xenopus* eggs (e.g., Charbonneau and Grey, 1984). Further, even in eggs, calcium elevation via fertilization or calcium ionophore treatment triggers neither compound exocytosis nor granule-granule fusion—the fusion event is strictly heterotypic, with the granules fusing with the PM. Thus the behavior seen after wounding is qualitatively different from what occurs in response to other stimuli, as expected if damage triggers a promiscuous fusion response of internal compartments. Second, cortical granules are not required for repair in later stages of *Xenopus* development, in that *Xenopus* blastomeres, which lack cortical granules, readily close PM disruptions (Clark *et al.*, 2009). Third, cell types that are commonly regarded as healing slowly, namely invertebrate neurons, display the same wound response hallmarks seen in fast-healing cells: calcium dependence (Yawo and Kuno, 1985), contraction at the wound edge (Krause *et al.*, 1994), and accumulation of vesicles at the site of damage (Eddleman *et al.*, 1997). Fourth, other aspects of the healing response, such as Rho GTPase–dependent assembly of actin filaments and myosin-2 at the wound site, are conserved across diverse phyla and cell types, both slow and fast healing (Sonnemann and Bement, 2011; Abreu-Blanco *et al.*, 2014). In addition, the pattern of dysferlin recruitment observed in this study is consistent with findings from muscle cells (e.g., Lek *et al.*, 2013; McDade *et al.*, 2014). Thus we suspect that at least some features of the response observed here will occur in other systems, albeit based on different pools of intracellular compartments.

We also provide evidence that calcium remains locally elevated for several minutes after wounding, confirming earlier reports that even cells that are able to quickly halt the influx of high–molecular weight dextrans nevertheless exhibit increased PM permeability to ions for minutes (Fein and Terasaki, 2005; Luxardi *et al.*, 2014). In transected axons, calcium concentrations at the cut edge remain elevated into the low millimolar range for approximately 1 min (Ziv and Spira, 1995) and elevated above physiological concentrations for >1 h (Eddleman *et al.*, 2000). Further, even in cultured mammalian cells, it has been reported that the wound remains open for several minutes (Jimenez *et al.*, 2014).

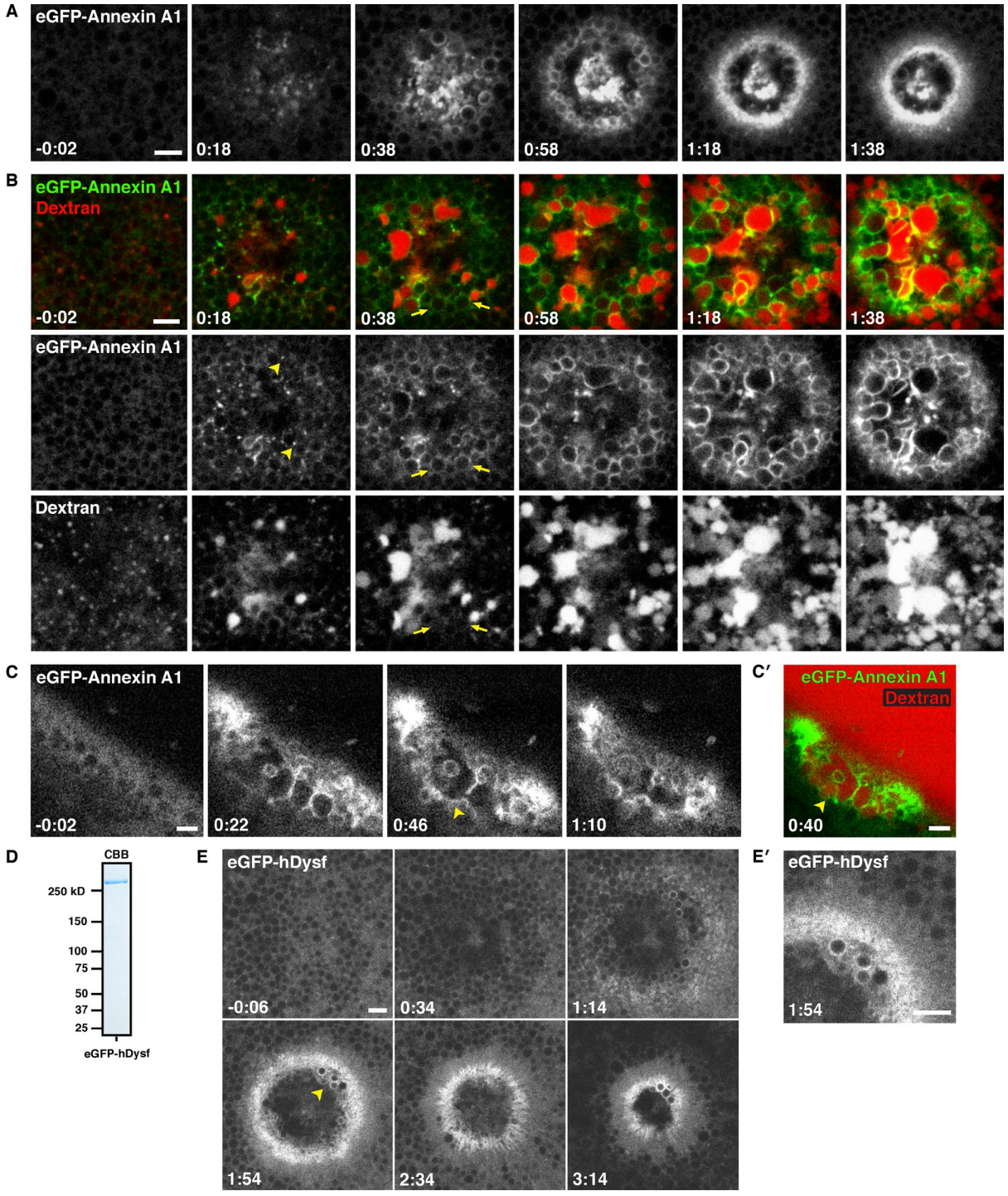

FIGURE 7: Human annexin A1 and dysferlin are recruited to membranous structures at wounds. (A) Low-magnification, en face view of wounded oocyte expressing eGFP-annexin A1. Annexin is recruited to cortical foci (0:18), vesicles at the wound edge (0:38), and a tight ring around the PM (1:18). See Supplemental Movie S14. (B) En face view of oocyte expressing eGFP-annexin A1 wounded in the presence of fluorescent extracellular dextran (Alexa Fluor 647 dextran). Annexin is recruited to foci (arrowheads) and vesicles before dextran incorporation (arrows). At increasing times postwounding, annexin also labels compartments in the wound interior (1:38). See Supplemental Movie S15. (C) Oblique view of a cell expressing eGFP-annexin A1 wounded in the presence of extracellular fluorescent dextran (not shown), showing eGFP-annexin A1 accumulating at a nascent patch (arrowheads). See Supplemental Movie S16. (C′) Still from C showing that eGFP-annexin A1–labeled compartments (green) fuse to form a barrier that excludes extracellular fluorescent dextran (red; Alexa Fluor 647 dextran) from the cytoplasm. (D) Coomassie-stained SDS–PAGE gel showing recombinant FLAG-eGFP-hDysferlin_isoform 1 purified from *Sf9* cells. (E) Oocyte wounded after microinjection with recombinant FLAG-eGFP-hDysferlin. (E′) Enlargement of region indicated by an arrowhead in E, showing recruitment of dysferlin to a tight ring at the PM bordering the wound and to vesicles at wound edge. Time in minutes:seconds, with $t = 0{:}00$ corresponding to the moment of wounding. Scale bars, 5 μm.

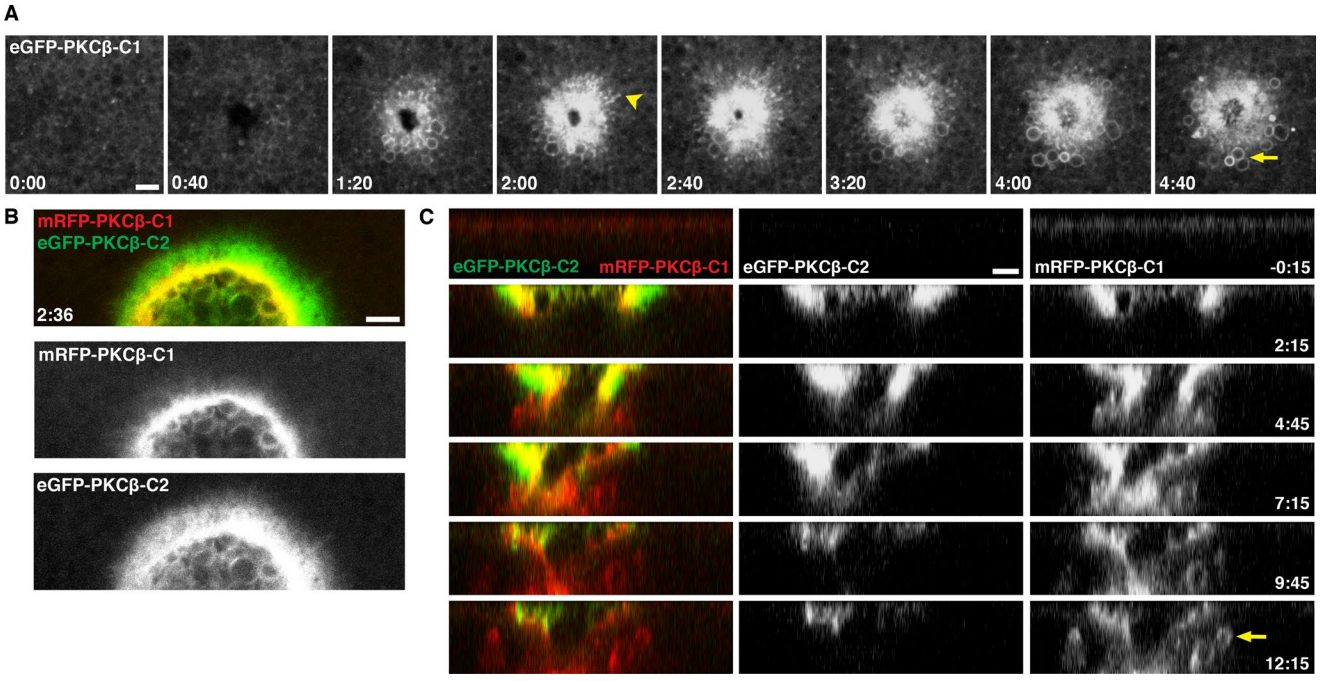

FIGURE 8: Wound-induced lipid domains persist throughout membrane repair. (A) En face view of wounded eGFP-PKCβ-C1–expressing oocyte. C1 labels both small (arrowhead at $t = 2:00$) and large (arrow at $t = 4:40$) membrane structures upon wounding. See Supplemental Movie S17. (B) Cells expressing mRFP-PKCβ-C1 and eGFP-PKCβ-C2 reveal lipid patterning around wounds. C1 accumulates at the leading edge of wounds, whereas C2 is more broadly distributed. See Supplemental Movie S18. (C) A *z*-view of membrane dynamics after wounding, as seen with mRFP-PKCβ-C1 and eGFP-PKCβ-C2. Remodeling of wound area and patch continues long after the initial membrane disruption and loss of C2, with C1 evident on the presumptive patch, as well as in vesicles surrounding the patch (arrow). See Supplemental Movie S19. Time in minutes:seconds, with $t = 0:00$ corresponding to the moment of wounding. Scale bar, 5 μm.

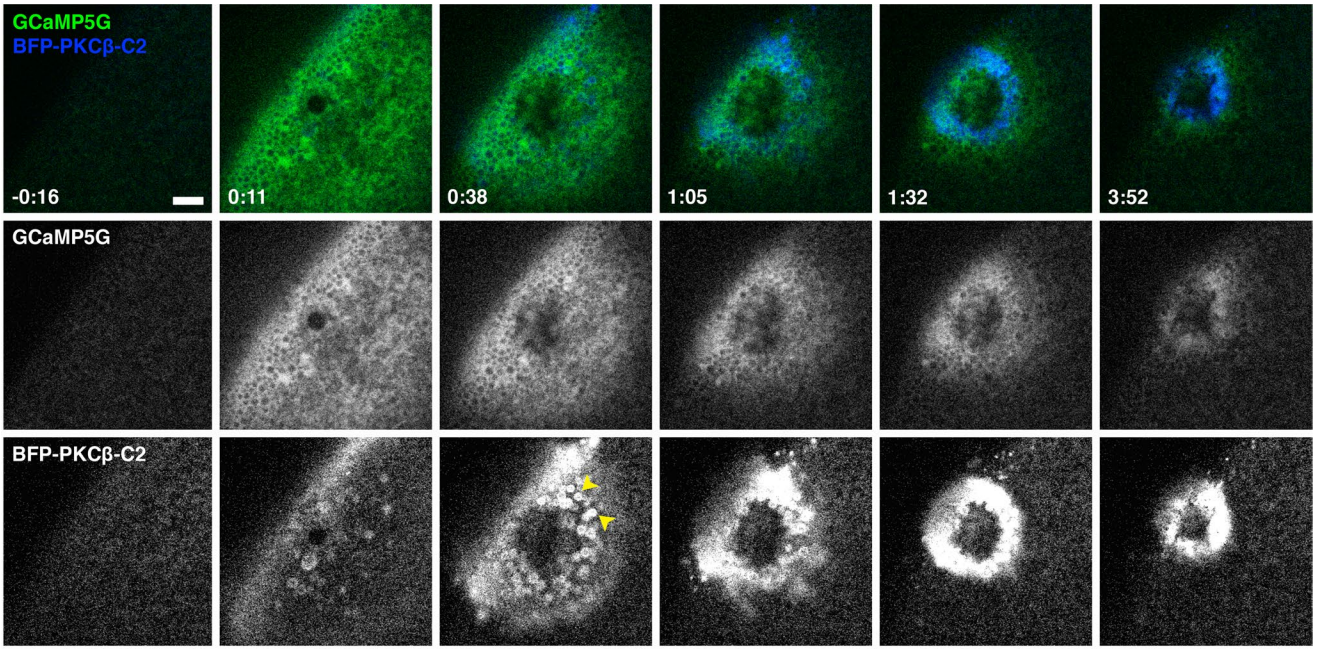

FIGURE 9: C2 accumulation follows elevation of intracellular calcium. Oblique view of wounded oocyte expressing GCaMP5G and BFP-PKCβ-C2. Increased calcium (detected by GCaMP5G) initially extends far from the site of membrane damage before being confined to a ring around the wound edge at later time points. The pattern of C2 recruitment follows that of calcium elevation, although the GCaMP5G signal is broader and more diffuse, whereas C2 is concentrated on the PM and vesicles (arrowheads). See Supplemental Movie S20. Time in minutes:seconds, with $t = 0:00$ corresponding to the moment of wounding. Scale bar, 10 μm.

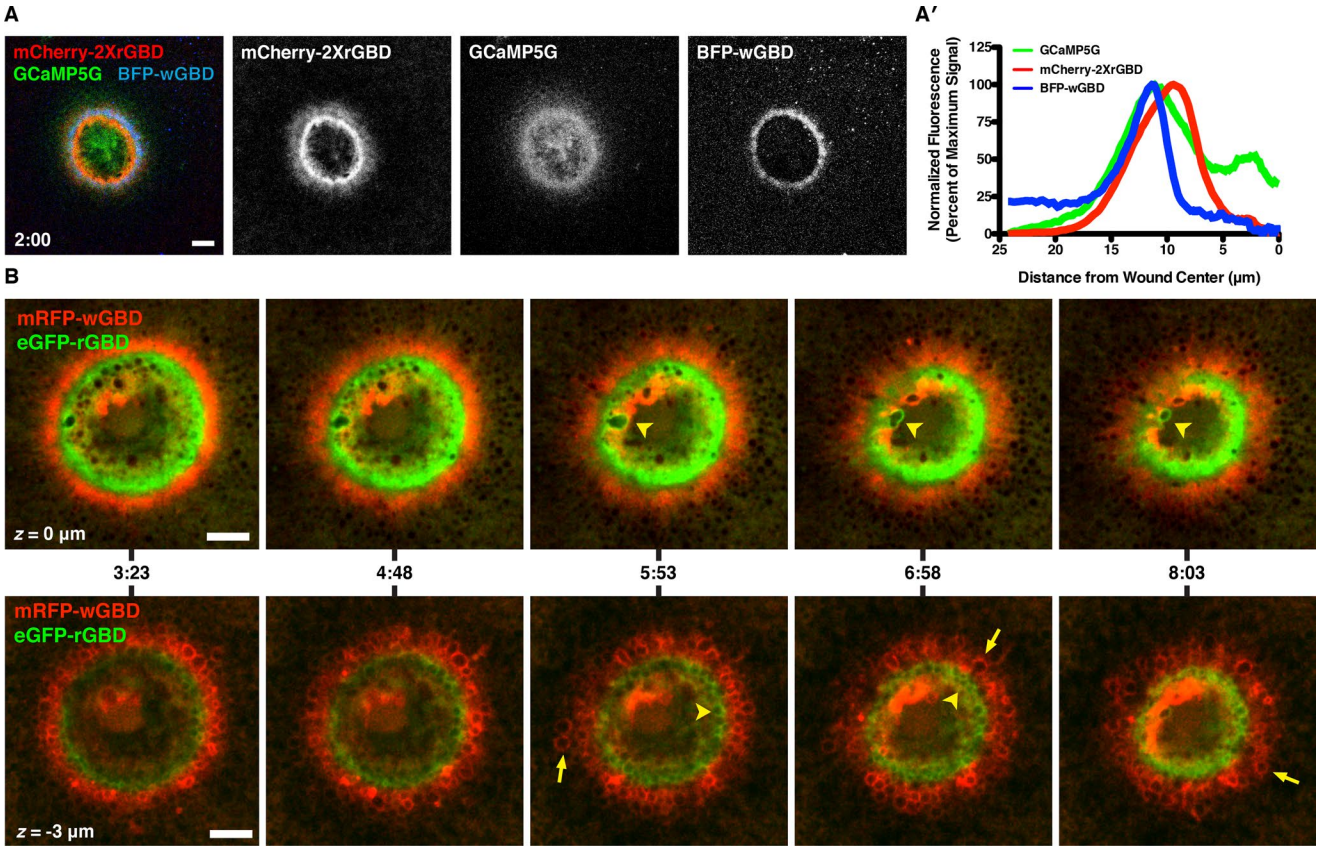

FIGURE 10: Patterning of elevated calcium, Rho, and Cdc42. (A) Low-magnification, en face view of wounded oocyte expressing BFP-wGBD, mCherry-2XrGBD, and GCaMP5G; the ring of calcium elevation overlaps the Rho and Cdc42 activity zones. See Supplemental Movie S21. (A′) Line scan from A, showing positions of active Rho and Cdc42 with respect to calcium. The increased calcium spans both zones, with peak intensity of the GCaMP5G signal closer to the peak of Cdc42 activity than that of Rho. (B) En face views of wounded oocyte expressing mRFP-wGBD and eGFP-rGBD from two different focal planes. $z = 0$ μm (top row, Supplemental Movie S22) corresponds to a surface view, whereas $z = -3$ μm (bottom row, Supplemental Movie S23) represents a subcortical view. Active Rho (arrowheads) and Cdc42 (arrows) are present on compartments other than the PM at wounds. Time in minutes:seconds, with $t = 0:00$ corresponding to the moment of wounding. Scale bars, 10 μm.

These observations are surprising, in that it has been assumed that if PM holes are not immediately and completely resealed, calcium inrush will rapidly kill the cell. However, our results show that after an initial "bloom" of calcium elevation triggered by wounding, the calcium signal rapidly shrinks back until it is tightly confined to a ring overlying the site where the Rho GTPases are active and the majority of the dramatic membrane dynamics are taking place. We suspect that this focusing reflects the remarkable capability of cells to sequester and buffer cytosolic calcium (Ziv and Spira, 1993; Allbritton *et al.*, 1992). If so, it follows that extensive vesicle cross-linking by membrane-associated proteins such as annexins (Blackwood and Ernst, 1990), dysferlin (Bansal *et al.*, 2003), MG53 (Cai *et al.*, 2009), or the enigmatic "tethering factor" (McNeil and McNeil, 2005) in parts of the wound may be sufficient to slow calcium influx to within the range of cellular buffering capacity. Consistent with this notion, we found that tightly packed vesicles appeared to serve as barriers to dextran diffusion in the cytoplasm. Further, we found that human annexin A1 is rapidly recruited to wound sites and extensively labels not only the PM, but also sites of vesicle–vesicle contact.

In this light, prolonged local elevation of calcium would be viewed as an important feature of the healing process rather than a sign and cause of incipient cell death. That is, protracted calcium elevation at the wound would be analogous to keeping steady pressure on a laceration, such that the calcium serves to drive vesicle fusion and/or aggregation to limit loss of material from the cell until the contractile array can be assembled and ingress to heal the defect. This idea is particularly appealing, in that calcium elevation is known to be the trigger for Rho GTPase activation (Benink and Bement, 2005; Abreu-Blanco *et al.*, 2014), and, as shown here, the calcium ring overlaps both the Rho and Cdc42 zone. Moreover, the calcium-dependent kinase PKCβ is required for proper organization of the Rho GTPase activity zones at wounds (Vaughan *et al.*, 2014). Because calcium is also known to drive the production of DAG (Kunkel *et al.*, 2007), a key determinant of PKCβ localization, it appears that postwound calcium serves as an initial signaling gradient from which subcellular patterns may be formed to assemble the factors needed to drive wound closure.

Our results also provide potential resolutions to two conceptual challenges imposed by the patch hypothesis: how the double-membrane compartment predicted by patching is converted into a single membrane and how a membrane patch derived from fusion of one or more intracellular compartments manages to serve as a functioning PM when (presumably) the proteins and lipids comprising the membranes of the intracellular compartments differ significantly from those of the PM. With respect to conversion of a double into a single membrane, the observation of explodosis provides a simple solution: rather than fusing with the PM (as in exocytosis), some of the patching-generated compartments rupture on their exoplasmic faces,

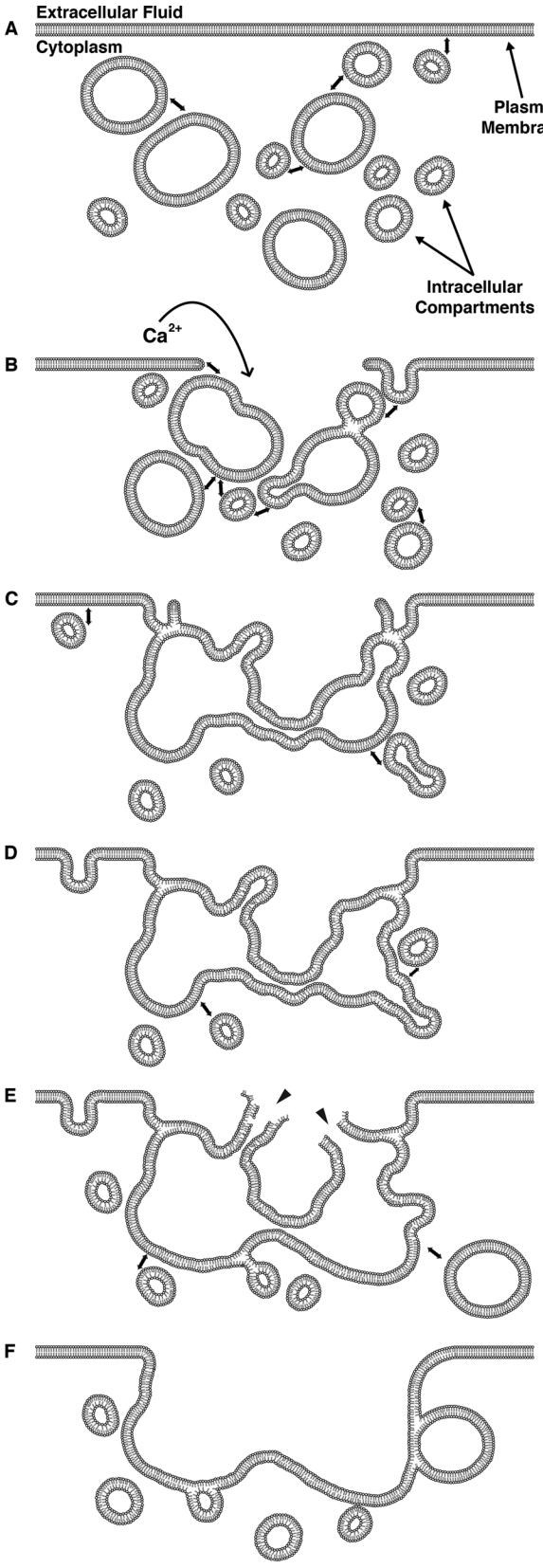

FIGURE 11: Schematic diagram of membrane dynamics at single-cell wounds. Representative time course of wound-induced membrane dynamics. (A) Resting plasma membrane with proximal intracellular membranous compartments. Double-headed arrows represent incipient membrane fusion events. Upon wounding (B), calcium enters the cell, causing fusion of intracellular vesicles with each other and the PM to form a patching membrane (C). Intracellular compartments continue to fuse with both the patch and the PM distal to the site of damage (D–F). The extracellular face of the patch ruptures outward (E; arrowheads) in a process called "explodosis"; this allows for resolution of a double-membrane structure and formation of a continuous barrier between the cytoplasm and the extracellular environment (F). Membrane fusion and remodeling events occur long after the initial resealing events.

leaving a single membrane. With respect to how a patching membrane provides a fully functional replacement for the PM, we suggest that it does not. Instead, we propose that the patching membrane is replaced via the extensive remodeling that begins almost as soon as it is formed and which, based on the results of DAG imaging, continues for 15 min or more after the initial damage. Such a mechanism could work alone or in conjunction with other mechanisms, such as scission mediated by endosomal sorting complex required for transport proteins (ESCRT; Jimenez *et al.*, 2014) or actomyosin-powered contraction (Sonnemann and Bement, 2011).

Finally, we add a technical observation to the effect that in spite of our efforts to be thorough in terms of probes and imaging regimes, we almost certainly missed many important events. We base this statement on the fact that essentially every probe we tried revealed something different about the healing process. Even the presumably inert dextran labeled not only compartments that fused with the PM, but also intensely stained mysterious structures that formed in the wound pit. We therefore assume that other sets of probes would reveal additional features of the healing process. Further, because we focused on membrane dynamics within the cell, the remarkable membranous elaborations seen using EM and other approaches (e.g., Bluemink, 1972; Jimenez *et al.*, 2014; Moe *et al.*, 2015; Figure 2) were largely ignored.

MATERIALS AND METHODS

Plasmids

The probes containing the C1 or C2 domains of *Xenopus laevis* PKCβ were generated as previously described (Yu and Bement, 2007). BFP-PKCβ-C2 was constructed by excising eGFP from eGFP-PKCβ-C2 using *Bam*HI and *Bsp*EI and replacing it with BFP. pCMV-GCaMP5G was a gift from Douglas Kim and Loren Looger (Janelia Research Campus, Howard Hughes Medical Institute; Addgene plasmid #31788). GCaMP5G was subcloned into pCS2+ with *Bam*HI and *Eco*RI. Human annexin A1 (accession number BC001275) was obtained from Open Biosystems (Huntsville, AL; clone 345615) and subcloned into eGFP-pCS2+ using *Bsp*E1 and *Xba*I. The probes for active GTPases—mRFP-wGBD and eGFP-rGBD—were generated as previously described (Sokac *et al.*, 2003; Benink and Bement, 2005). BFP-wGBD was constructed by excising monomeric red fluorescent protein (mRFP) from mRFP-wGBD using *Bam*HI and *Bsp*EI and replacing it with BFP. mCherry-2xrGBD was constructed by adding an additional rGBD between the *Bsp*EI and *Xho*I sites of mCherry-rGBD. Human dysferlin isoform 1 (accession number NM_003494.3) was obtained from the Jain Foundation (www.jain-foundation.org/) and subcloned into eGFP-pCS2+. A FLAG sequence was added by PCR to the N-terminus of eGFP, and the resultant FLAG-eGFP-hDysf construct was subcloned into pFastBac1 using *Not*I.

Oocyte acquisition and preparation

Ovarian tissue was procured from *X. laevis* females via surgical procedures approved by the University of Wisconsin–Madison Institutional Animal Care and Use Committee. Tissue was stored in 1× modified Barth's solution (88 mM NaCl, 1 mM KCl, 2.4 mM $NaHCO_3$, 0.82 mM

$MgSO_4$, 0.33 mM $NaNO_3$, 0.41 mM $CaCl_2$, and 10 mM 4-(2-hydroxyethyl)-1-piperazineethanesulfonic acid [HEPES], pH 7.4, supplemented with 100 µg/ml gentamicin sulfate, 6 µg/ml tetracycline, and 25 µg/ml ampicillin) at 16–18°C. Follicle cells were removed from oocytes by enzymatic digestion (8 mg/ml type I collagenase [Life Technologies, Grand Island, NY] in 1× Barth's for 1 h at 16–18°C on a 60-rpm rotating plate), followed by manual dissociation with fine forceps. Defolliculated oocytes were stored in 1× Barth's (changed daily) until use.

mRNA preparation and oocyte microinjection

mRNAs were transcribed in vitro using the mMessage mMachine SP6 Transcription Kit (Life Technologies), followed by purification using RNeasy Mini Kit (Qiagen, Hilden, Germany) per manufacturer's instructions. Transcript size was verified on 1% agarose/formaldehyde denaturing gels versus Millennium Marker (Life Technologies) molecular weight standard. Oocytes were injected while in 1× Barth's with a 40-nl injection volume. Cells were allowed to recover at least 30 min between injections. Probes for active GTPases (wGBDs and rGBDs) were each injected at a final needle concentration of 125–167 µg/ml. eGFP-annexinA1 was injected at 50–100 µg/ml. GCaMP5G was injected at 125 µg/ml. eGFP- and BFP-PKCβ C2 were injected at 50 µg/ml. eGFP- and mRFP-PKCβ C1 was injected at 250–500 µg/ml. FLAG-eGFP-hDysf was injected at 1.5 µM, corresponding to a needle concentration of 400 µg/ml. Injected oocytes were stored in 1× Barth's at 16–18°C and mRNAs allowed to express for 24 h before imaging. Oocytes injected with FLAG-eGFP-hDysferlin were allowed to recover for at 24 h before imaging.

Cell labeling

Cellular membranes were labeled by 30–60 min of preincubation with octadecyl rhodamine B chloride (R18) or FM1-43 at 1 or 5–20 µM in 1× Barth's, respectively. Fluorescent dextrans were added to 1× Barth's, at 10–100 µM final concentration at 10–60 min before wounding; dextran sizes were 3000 Da (Texas Red dextran) or 10,000 Da (Oregon Green 488 and Alexa Fluor 647 dextrans).

Purification of recombinant proteins from insect cells

Dysferlin constructs in pFastBac1 were transformed into DH10Bac-competent *Escherichia coli* (Thermo Fisher Scientific, Carlsbad, CA) and positive clones selected by blue/white screening. Recombinant bacmids were isolated and subsequently transfected into *Sf9* cells using Cellfectin II reagent (Thermo Fisher Scientific). Highly expressing clones were selected and virus amplified for two additional generations. *Sf9* cells (2.2×10^7 per plate) were infected with high-titer baculovirus and allowed to incubate for 72 h at 27°C. Infected cells were collected by centrifugation (5 min at 500 × *g*) and stored at –80°C until protein purification.

Baculovirus-infected *Sf9* cell pellets were resuspended in five volumes of solubilization buffer (1× phosphate-buffered saline [PBS], pH 7.5, 1% [vol/vol] Triton X-100, 0.5 µg/ml leupeptin, 0.5 µg/ml aprotinin, 0.5 µg/ml pepstatin A, 40 µg/ml phenylmethylsulfonyl fluoride [PMSF], 100 µg/ml benzamidine, 0.5 µg/ml E64) and incubated at 4°C for 1 h with gentle end-over-end mixing. Lysates were clarified by centrifugation at 21,100 × *g* for 15 min. The supernatant was incubated in batch format with anti–FLAG-M2 agarose beads (Sigma-Aldrich, St. Louis, MO) for 1 h at 4°C before being added to a column. The column was washed with 3 × 10 column volumes of wash buffer (1× PBS, pH 7.5, 40 µg/ml PMSF, 100 µg/ml benzamidine), and recombinant protein was eluted with 1 M arginine, pH 4.4, into an equal volume of collection buffer (50 mM HEPES, pH 8.5, 200 mM KCl, 80 µg/ml, PMSF, 200 µg/ml, benzamidine). Elution fractions were separated by SDS–PAGE (4–12% gradient gel), followed by Coomassie brilliant blue staining. Desired fractions were pooled and concentrated using 100K MWCO Amicon Ultra-15 filters (Millipore, Carrigtwohill, Ireland). The buffer was exchanged in-filter to remove residual arginine to final conditions compatible with downstream applications (25 mM HEPES, pH 7.5, 100 mM KCl, 10% glycerol). The purity and concentration of the recombinant proteins were determined by SDS–PAGE and BCA Assay (Pierce, Rockford, IL), respectively. Aliquots were snap-frozen in liquid nitrogen before storage at –80°C.

Image acquisition, wounding, and data analysis

Laser scanning and swept field confocal microscopy was performed using Nikon Eclipse Ti inverted microscopes and Nikon 60X CFI Plan APO oil objectives (1.4 numerical aperture) with either a Prairie Point Scanner or an Opterra Multipoint confocal system (Bruker, Middleton, WI). Cells were wounded with illumination from a 488-nm uncaging laser (Bruker) or 440-nm dye laser setup pumped by a MicroPoint 337-nm nitrogen laser (Andor, South Windsor, CT). The wounding laser is nominally diffraction limited and manually activated for ~1 s with a ~5- to 10-Hz repetition rate, and the source laser (per manufacturer specifications) has a maximal output of 400 µJ/pulse. Imaging data were processed using Fiji (Schindelin *et al.*, 2012) and Volocity (PerkinElmer, Waltham, MA). The line scan in Figure 10A′ was made in Fiji by performing a radial reslice around the wound center and making an average intensity projection of the resultant stack. The fluorescence intensity along the line extending from the wound center was plotted in Prism 5 (GraphPad, La Jolla, CA). Each channel was normalized such that the maximum and minimum fluorescence intensity values for that channel became 100 and 0%, respectively. All of the results reported here were representative of 20 to >100 wounds. Moreover, the membrane behaviors reported here, including exocytosis, patching, and explodosis, were repeatedly observed with three to five different probes (e.g., exocytosis was revealed by dextrans, FM 1-43, wGBD, and rGBD; patching was strongly revealed by C2, C1, and GFP-annexin and weakly revealed by R18; and explodosis was revealed by C2, C1, GFP-annexin, and wGBD). Thus, although we cannot exclude the possibility that some probes (e.g., dextran) altered the wound response in some way, we can say with confidence that none of these behaviors was a consequence of having a particular probe (e.g., dextran) present during wounding.

ACKNOWLEDGMENTS

This work was supported by National Institutes of Health Grant GM52932 to W.M.B. and National Research Service Award GM07215 to N.R.D. K.J.S. is supported by the Jain Foundation. We acknowledge National Institutes Health Grant R44 MH065724 to K.W.E and are extremely grateful for the support of the Bruker Corporation for on-site demonstrations and training on the Opterra. A portion of these results was initially presented during the 2014 Celldance Exhibit at the American Society for Cell Biology (ASCB) Annual Meeting. The video entitled Cell Repair can be found on the ASCB website (www.ascb.org/). We thank the ASCB's Public Information Committee for funding, technical support, and the opportunity to share our work.

REFERENCES

Abreu-Blanco MT, Verboon JM, Parkhurst SM (2011). Cell wound repair in Drosophila occurs through three distinct phases of membrane and cytoskeletal remodeling. J Cell Biol 193, 455–464.

Abreu-Blanco MT, Verboon JM, Parkhurst SM (2014). Coordination of Rho family GTPase activities to orchestrate cytoskeleton responses during cell wound repair. Curr Biol 24, 144–155.

Akerboom J, Chen TW, Wardill TJ, Tian L, Marvin JS, Mutlu S, Calderón NC, Esposti F, Borghuis BG, Sun XR, *et al*. (2012). Optimization of a GCaMP calcium indicator for neural activity imaging. J Neurosci 32, 3819–3840.
Allbritton NL, Meyer T, Stryer L (1992). Range of messenger action of calcium ion and inositol 1,4,5-trisphosphate. Science 258, 1812–1815.
Andrews NW, Perez F (2015). The plasma membrane repair shop: fixing the damage. Semin Cell Dev Biol 45, 1.
Bansal D, Miyake K, Vogel SS, Groh S, Chen CC, Williamson R, McNeil PL, Campbell KP (2003). Defective membrane repair in dysferlin-deficient muscular dystrophy. Nature 423, 168–172.
Bembenek JN, Richie CT, Squirrell JM, Campbell JM, Eliceiri KW, Poteryaev D, Spang A, Golden A, White JG (2007). Cortical granule exocytosis in C. elegans is regulated by cell cycle components including separase. Development 134, 3837–3848.
Bement WM (1992). Signal transduction by calcium and protein kinase C during egg activation. J Exp Zool 263, 382–397.
Bement WM, Mandato CA, Kirsch MN (1999). Wound-induced assembly and closure of an actomyosin purse string in Xenopus oocytes. Curr Biol 9, 579–587.
Benink HA, Bement WM (2005). Concentric zones of active RhoA and Cdc42 around single cell wounds. J Cell Biol 168, 429–439.
Bi GQ, Alderton JM, Steinhardt RA (1995). Calcium-regulated exocytosis is required for cell membrane resealing. J Cell Biol 131, 1747–1758.
Blackwood RA, Ernst JD (1990). Characterization of Ca2(+)-dependent phospholipid binding, vesicle aggregation and membrane fusion by annexins. Biochem J 266, 195–200.
Bluemink JG (1972). Cortical wound healing in the amphibian egg: an electron microscopical study. J Ultrastruct Res 41, 95–114.
Cai C, Masumiya H, Weisleder N, Matsuda N, Nishi M, Hwang M, Ko JK, Lin P, Thornton A, Zhao X, *et al*. (2009). MG53 nucleates assembly of cell membrane repair machinery. Nat Cell Biol 11, 56–64.
Campanella C, Andreuccetti P (1977). Ultrastructural observations on cortical endoplasmic reticulum and on residual cortical granules in the egg of Xenopus laevis. Dev Biol 56, 1–10.
Castellano-Muñoz M, Peng AW, Salles FT, Ricci AJ (2012). Swept field laser confocal microscopy for enhanced spatial and temporal resolution in live-cell imaging. Microsc Microanal 18, 753–760.
Charbonneau M, Grey RD (1984). The onset of activation responsiveness during maturation coincides with the formation of the cortical endoplasmic reticulum in oocytes of Xenopus laevis. Dev Biol 102, 90–97.
Clark AG, Miller AL, Vaughan E, Yu H-YE, Penkert R, Bement WM (2009). Integration of single and multicellular wound responses. Curr Biol 19, 1389–1395.
Cooper ST, McNeil PL (2015). Membrane repair: mechanisms and pathophysiology. Physiol Rev 95, 1205–1240.
Eddleman CS, Ballinger ML, Smyers ME, Godell CM, Fishman HM, Bittner GD (1997). Repair of plasmalemmal lesions by vesicles. Proc Natl Acad Sci USA 94, 4745–4750.
Eddleman CS, Bittner GD, Fishman HM (2000). Barrier permeability at cut axonal ends progressively decreases until an ionic seal is formed. Biophys J 79, 1883–1890.
Fein A, Terasaki M (2005). Rapid increase in plasma membrane chloride permeability during wound resealing in starfish oocytes. J Gen Physiol 126, 151–159.
Gingell D (1970). Contractile responses at the surface of an amphibian egg. J Embryol Exp Morphol 23, 583–609.
Heilbrunn LV (1928). The Colloid Chemistry of Protoplasm, Berlin: Gebrüder Borntraeger.
Howard AC, McNeil AK, Xiong F, Xiong W-C, McNeil PL (2011). A novel cellular defect in diabetes: membrane repair failure. Diabetes 60, 3034–3043.
Idone V, Tam C, Goss JW, Toomre D, Pypaert M, Andrews NW (2008). Repair of injured plasma membrane by rapid Ca2+-dependent endocytosis. J Cell Biol 180, 905–914.
Jimenez AJ, Maiuri P, Lafaurie-Janvore J, Divoux S, Piel M, Perez F (2014). ESCRT machinery is required for plasma membrane repair. Science 343, 1247136.
Kohout SC, Corbalán-García S, Torrecillas A, Goméz-Fernandéz JC, Falke JJ (2002). C2 domains of protein kinase C isoforms alpha, beta, and gamma: activation parameters and calcium stoichiometries of the membrane-bound state. Biochemistry 41, 11411–11424.
Krause TL, Fishman HM, Ballinger ML, Bittner GD (1994). Extent and mechanism of sealing in transected giant axons of squid and earthworms. J Neurosci 14, 6638–6651.
Kunkel MT, Toker A, Tsien RY, Newton AC (2007). Calcium-dependent regulation of protein kinase D revealed by a genetically encoded kinase activity reporter. J Biol Chem 282, 6733–6742.
Labazi M, McNeil AK, Kurtz T, Lee TC, Pegg RB, Angeli JPF, Conrad M, McNeil PL (2015). The antioxidant requirement for plasma membrane repair in skeletal muscle. Free Radic Biol Med 84, 246–253.
Lek A, Evesson FJ, Lemckert FA, Redpath GM, Lueders AK, Turnbull L, Whitchurch CB, North KN, Cooper ST (2013). Calpains, cleaved mini-dysferlinC72, and L-type channels underpin calcium-dependent muscle membrane repair. J Neurosci 33, 5085–5094.
Lennon NJ, Kho A, Bacskai BJ, Perlmutter SL, Hyman BT, Brown RH Jr (2003). Dysferlin interacts with annexins A1 and A2 and mediates sarcolemmal wound-healing. J Biol Chem 278, 50466–50473.
Luxardi G, Reid B, Maillard P, Zhao M (2014). Single cell wound generates electric current circuit and cell membrane potential variations that requires calcium influx. Integr Biol (Camb) 6, 662–672.
Mandato CA, Bement WM (2001). Contraction and polymerization cooperate to assemble and close actomyosin rings around Xenopus oocyte wounds. J Cell Biol 154, 785–797.
McDade JR, Archambeau A, Michele DE (2014). Rapid actin-cytoskeleton-dependent recruitment of plasma membrane-derived dysferlin at wounds is critical for muscle membrane repair. FASEB J 28, 3660–3670.
McNeil A, McNeil PL (2005). Yolk granule tethering: a role in cell resealing and identification of several protein components. J Cell Sci 118, 4701–4708.
McNeil AK, Rescher U, Gerke V, McNeil PL (2006). Requirement for annexin A1 in plasma membrane repair. J Biol Chem 281, 35202–35207.
McNeil PL, Ito S (1989). Gastrointestinal cell plasma membrane wounding and resealing in vivo. Gastroenterology 96, 1238–1248.
McNeil PL, Miyake K, Vogel SS (2003). The endomembrane requirement for cell surface repair. Proc Natl Acad Sci USA 100, 4592–4597.
McNeil PL, Vogel SS, Miyake K, Terasaki M (2000). Patching plasma membrane disruptions with cytoplasmic membrane. J Cell Sci 113, 1891–1902.
Miyake K, McNeil PL (1995). Vesicle accumulation and exocytosis at sites of plasma membrane disruption. J Cell Biol 131, 1737–1745.
Moe AM, Golding AE, Bement WM (2015). Cell healing: calcium, repair and regeneration. Semin Cell Dev Biol 45, 18–23.
Ponomareva OY, Eliceiri KW, Halloran MC (2016). Charcot-Marie-Tooth 2b associated Rab7 mutations cause axon growth and guidance defects during vertebrate sensory neuron development. Neural Dev 11, 2.
Potez S, Luginbühl M, Monastyrskaya K, Hostettler A, Draeger A, Babiychuk EB (2011). Tailored protection against plasmalemmal injury by annexins with different Ca2+ sensitivities. J Biol Chem 286, 17982–17991.
Reddy A, Caler EV, Andrews NW (2001). Plasma membrane repair is mediated by Ca(2+)-regulated exocytosis of lysosomes. Cell 106, 157–169.
Ridley AJ (2006). Rho GTPases and actin dynamics in membrane protrusions and vesicle trafficking. Trends Cell Biol 16, 522–529.
Schindelin J, Arganda-Carreras I, Frise E, Kaynig V, Longair M, Pietzsch T, Preibisch S, Rueden C, Saalfeld S, Schmid B, *et al*. (2012). Fiji: an open-source platform for biological-image analysis. Nat Methods 9, 676–682.
Sokac AM, Co C, Taunton J, Bement W (2003). Cdc42-dependent actin polymerization during compensatory endocytosis in Xenopus eggs. Nat Cell Biol 5, 727–732.
Sonnemann KJ, Bement WM (2011). Wound repair: toward understanding and integration of single-cell and multicellular wound responses. Annu Rev Cell Dev Biol 27, 237–263.
Steinhardt RA, Bi G, Alderton JM (1994). Cell membrane resealing by a vesicular mechanism similar to neurotransmitter release. Science 263, 390–393.
Swaggart KA, Demonbreun AR, Vo AH, Swanson KE, Kim EY, Fahrenbach JP, Holley-Cuthrell J, Eskin A, Chen Z, Squire K, *et al*. (2014). Annexin A6 modifies muscular dystrophy by mediating sarcolemmal repair. Proc Natl Acad Sci USA 111, 6004–6009.
Terasaki M, Miyake K, McNeil PL (1997). Large plasma membrane disruptions are rapidly resealed by Ca2+-dependent vesicle-vesicle fusion events. J Cell Biol 139, 63–74.
Vaughan EM, You J-S, Yu H-YE, Lasek A, Vitale N, Hornberger TA, Bement WM (2014). Lipid domain–dependent regulation of single-cell wound repair. Mol Biol Cell 25, 1867–1876.
Yawo H, Kuno M (1985). Calcium dependence of membrane sealing at the cut end of the cockroach giant axon. J Neurosci 5, 1626–1632.
Yu H-YE, Bement WM (2007). Control of local actin assembly by membrane fusion-dependent compartment mixing. Nat Cell Biol 9, 149–159.
Ziv NE, Spira ME (1993). Spatiotemporal distribution of Ca2+ following axotomy and throughout the recovery process of cultured Aplysia neurons. Eur J Neurosci 5, 657–668.
Ziv NE, Spira ME (1995). Axotomy induces a transient and localized elevation of the free intracellular calcium concentration to the millimolar range. J Neurophysiol 74, 2625–2637.